JOURNAL OF MATERIALS SCIENCE **35** (2000) 583–592

The transverse compression of PPTA fibers

Part II *Fiber transverse structure*

J. SINGLETARY*, H. DAVIS†, Y. SONG
College of Textiles, North Carolina State University, Box 8301, Raleigh, North Carolina, USA 27695-8301
E-mail: hdavis@tx.ncsu.edu

M. K. RAMASUBRAMANIAN
College of Wood and Paper Science, North Carolina State University, Raleigh, North Carolina, USA

W. KNOFF
DuPont de Nemours and Co., Inc., Advanced Fibers Systems, Richmond, Virginia, USA

The single fiber transverse compression test (SFTCT) is applied to KEVLAR and TWARON poly (*para*-phenyleneterephthalamide) fibers, both continuous filament and staple, and of varying denier and heat-treatment, as well as M5 rigid-rod fibers. Resulting force-deflection curves are analyzed by a Hertzian contact model, to give the effective transverse modulus, and estimate the stress state in the fiber at the onset of yield. Confocal microscopy and finite element simulation are used in conjunction with SFTCT to describe the inelastic, transverse deformation of PPTA. The effects of skin-core structure and anisotropy in the fiber cross-section are discussed.

1. Introduction

In a related paper [1], we presented a device for the single fiber transverse compression test (SFTCT), applied to fine, highly anisotropic polymer fibers, and examined the accuracy of assumptions of test conditions made in analysis. These fibers have several applications in which transverse compression is important, such as cut-resistant and ballistic cloth [2], cables [3], and bolted composite panels. The structural engineering of such applications requires characterizing both elastic and inelastic transverse compression. The engineering of fibers for these applications requires experimental evidence of the structure-property relations that affect fiber transverse compression.

In this paper, we address both these needs. We begin with a brief discussion of the structure of poly(*para*-phenyleneterephthalamide) (PPTA) fibers. We then present SFTCT data for PPTA fibers—Dupont's KEVLAR and Akzo Nobel's TWARON—from continuous filament and staple fibers, as well as experimental M5 rigid-rod fibers from Akzo Nobel [4–6]. Laser-scanning confocal microscopy (LSCM) and finite element (FE) simulation are used to examine the yield process of PPTA fibers in transverse compression. We close by discussing connections between fiber transverse compressive response and radially-dependent structure, as well as in-plane anisotropy.

1.1. PPTA fiber structure

PPTA fibers have a complex and long-studied structure (some reviews are given in [7–10]). Research on fiber structure has focused mainly on its effect on axial stiffness and strength, linking these to structural details such as chain and segregation [11, 12] and axial alignment. Less attention has been given to the influence of fiber structure on transverse mechanical response. From experience with fiber-reinforced plastics and other, highly anisotropic materials, we expect crystalline orientation to have little influence on transverse properties in highly-oriented fibers such as PPTA, indeed, analysis of the SFTCT loading suggests transverse compressive response of highly-anisotropic fibers is essentially independent of any out-of-plane properties for fibers in which $E_l \gg E_t$ [2, 13]. Therefore, the structural details which most affect transverse compressive response in PPTA fibers should be those of the cross-section. Fig. 1 is a model of the PPTA cross-sectional structure, adopted from Yabuki *et al.* [14, 15], which shows important features of the PPTA fiber cross-section in the literature:

1. PPTA fibers are reported to be composed of smaller fibrils, which are roughly circular cylinders, with diameters around 30–50 nm [11, 16, 17].

* *Present address*: 3TEX Engineered Fiber Products, 109 MacKenan Drive, Cary, NC 27511.

† Author to whom all correspondence should be addressed.

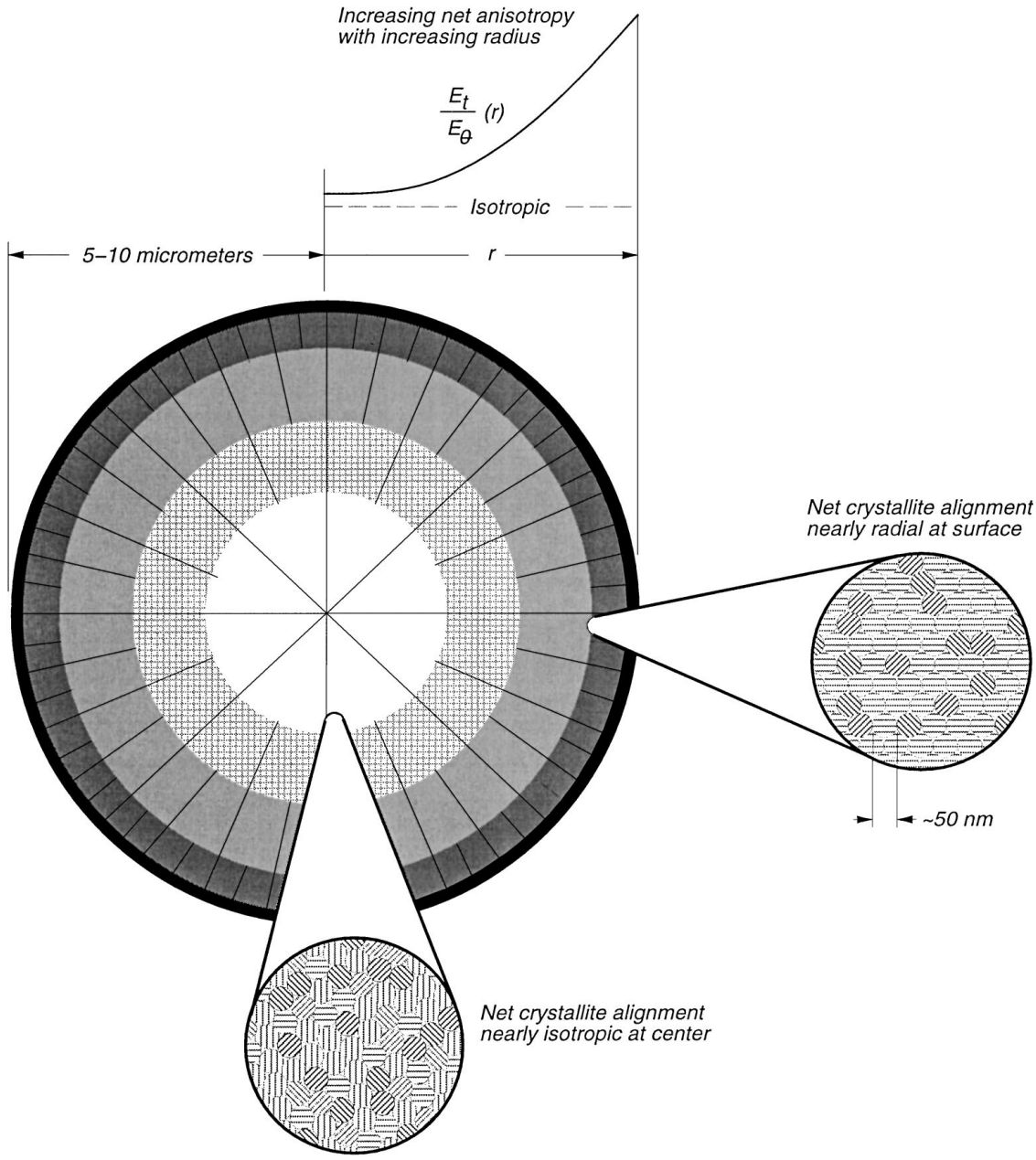

Figure 1 Model of the cross-section of PPTA fibers, adopted from Yabuki *et al.* (1976).

2. Between the fibrils are narrow regions of less order, possibly from crystalline misregister, quenching impurities [18], trapped water [19] and/or voids [20, 21], along which PPTA is expected to fibrillate.

3. Since the fibers are highly oriented and PPTA crystals pseudo-orthorhombic [9], the cross-section corresponds approximately to the *ab*-crystal plane, with the *a*-crystal direction more compliant than the *b*-direction, which is roughly parallel to hydrogen bonds [22–24].

4. Coagulation causes hydrogen bond planes to orient increasingly parallel to the radial direction, r, as radius increases. The fiber is thus closer to a transversely isotropic material at the center, and more anisotropic at the surface. This continuous radial gradient of fiber structure [25] has often been characterized as a discrete composite of 'sheath' and 'core' for convenience [16, 11, 26, 20, 21, 17], however, such discretization is not strictly correct [25, 27].

Although there is still little literature on M5 fibers, much of its cross-sectional structure parallels PPTA, including fibrillar structure and radially oriented hydrogen bond directions [28].

2. Theory

We refer to equations and analysis discussed in [1]. Transverse yield of polymer fibers has been characterized only qualitatively. For all but highly heat-treated fibers [29], PPTA deforms ductilely in transverse compression. Phoenix and Skelton [2] hypothesized that transverse yield in PPTA, PET and nylon fibers was dominated by the maximum resolved shear stress, $\tau_{\max}$, and estimated $\tau_{\max}$ at the onset of yield in SFTCT experiments. Batra and Nuruzzaman [30] reached similar conclusions about PET and nylon monofilaments, suggesting a Tresca yield criterion. Kotani *et al.* [31]

had limited success simulating HMPE monofilaments in SFTCT with a FE model assuming elastic-plastic behavior.

Extreme anisotropy of PPTA and similar fibers make elastic transverse deformation essentially independent of axial or torsional properties [2, 3, 13, 1]. Since the highest stresses developed at yield in the transverse compression of PPTA fibers [32] are much less than even the comparatively low axial compressive strength of PPTA [33], it is reasonable to assume that by extension, transverse inelastic deformation is also essentially independent of axial properties.

3. Procedures

3.1. Transverse compression experiments

We performed SFTCT on 1.5 and 6.0 denier[1] KEVLAR 29 continuous filament fibers, 1.5, 2.25, 4.2 and 6.0 denier KEVLAR 29 staple fibers, 1.5 denier TWARON 1000, 1055 and 2200, and both un-heat-treated and heat-treated M5 fibers, using the method described in [1]. Fibers were loaded quasi-statically, at a speed fast enough to neglect viscous response [34], and except for samples examined by LSCM (Section 3.2 below), were loaded to the limit of the SFTCT device, corresponding to $e \approx 45$–80%, depending on fiber stiffness and diameter. All fibers were loaded along lengths of 2–7 fiber diameters, which should be sufficient to approximate plane strain compression [1]. 20–40 fibers of each type were tested. The analysis used to calculate effective, transverse modulus, E_t, apparent strain at yield e_y, and maximum resolved shear stress at yield, τ_{max}, are summarized in [1]. The relation between E_t and platen travel, U_y, is [13]:

$$U_y = \frac{4F}{\pi E_t}\left[0.19 + \operatorname{arcsinh}\left(\sqrt{\frac{\pi R E_t}{4F}}\right)\right] \qquad (1)$$

where F is the force per unit length applied to the fiber, and R is the fiber radius.

3.2. Laser-scanning confocal microscopy

Some fibers were compressed to varying levels of inelastic compression, then unloaded, removed from the SFTCT device, and examined with LSCM. LSCM allows fiber cross-sections to be imaged without physically sectioning the fiber, which damages the cross-sections of highly anisotropic fibers such as PPTA even when great care is used (cf. [20, 21]). LSCM uses pinhole apertures at the light source and before the detector, reducing focal depth and increasing resolution. Reduced focal depth allows the microscope to discriminate views at differing depths in the y-direction (see [1] for explanation of directions). By scanning incrementally through y, then digitally composing the images, a view of the cross-section can be formed.

[1] *Denier* is a traditional textile measure of the inverse of lineal density of a fiber or yarn. Denier is the number of kilograms of fiber or yarn in 9 km, therefore, as denier increases, fiber diameter increases. For PPTA fibers, which are circular and have a specific gravity of 1.45, 1.5 denier corresponds to 12 μm average diameter; 6 denier corresponds to 24 μm average diameter.

We used a LEICA DM-RBE TCS-N/T confocal microscope. 6.0 denier KEVLAR 29 fibers (24 μm nominal diameter) were used, to give a large image. Six fibers were imaged: two undamaged, two compressed to $e \approx 25\%$ and two compressed to $e \approx 45\%$. A 488 nm argon laser provided illumination, and the image was filtered by a dichroic mirror with a 500 nm threshold. LSCM requires fluorescence for imaging, often from fluorescent dyes. We found the weak self-fluorescence of PPTA fibers gave clearer images than fluorescing dyes; images presented here are from self-fluorescence.

3.3. Finite element simulation

Inelastic deformation during SFTCT cannot be accounted for by elastic, Hertzian contact models [2, 13], and was instead simulated by FE models of the test. The models were used to reproduce individual SFTCT force-deflection curves for 1.5 denier KEVLAR 29. Experimental SFTCT force-deflection data was simulated by assuming a plasticity model, then iteratively adjusting the plastic parameters until the experimental force-deflection curve was repredicted.

Plane strain models of a transversely isotropic, circular cylinder, compressed between two parallel, stiff platens were built in ANSYS 5.0A–5.3 [35], using a range of meshing schemes and mesh densities. Symmetry allowed a model of only one quarter of the fiber and one half of one platen, with no displacement allowed across the symmetry boundaries. Fig. 2 shows a FE model. Linear elements were used, per the software's recommendations for contact problems [36]. The platen was prescribed to move incrementally lower, contacting and then incrementally deforming the fiber. Models with 300–2500 degrees of freedom (DOF) in the fiber were examined (the platen itself was more coarsely meshed), to check for mesh convergence. Predicted stresses in the fiber cross-section were negligibly affected by mesh changes for mesh densities of DOF > 700; predicted force-deflection curve were hardly sensitive to mesh changes or density.

The platen was assumed two orders of magnitude stiffer than the fiber, reasonable for the silicon platens used [37]. Software limitations prevented inelastic deformation for anisotropic materials (cf. [31]), therefore, following the observation [2, 3, 1] that plane strain transverse compression of highly anisotropic fibers is essentially independent of out-of-plane properties, we assumed the Poisson ratio equaled the in-plane Poisson ratio of KEVLAR 29, $\nu_{tt} = 0.43$ [33]. E_t and R came from the Hertzian analysis of the individual tests. (To verify the assumption of isotropy, FE simulations of elastic response of isotropic fibers were compared to simulations of a transversely isotropic fiber, using the elastic constants of KEVLAR 29 reported in [33]. As expected, anisotropy negligibly affected the predicted in-plane stress state or force-deflection curve.) We assumed a von Mises yield criterion, using an isotropic hardening rule. The von Mises stress criterion and post-yield tangent modulus, $E_{t,tan}$, were determined by iteratively comparing simulated force-deflection curves with the specific experimental force-deflection curve.

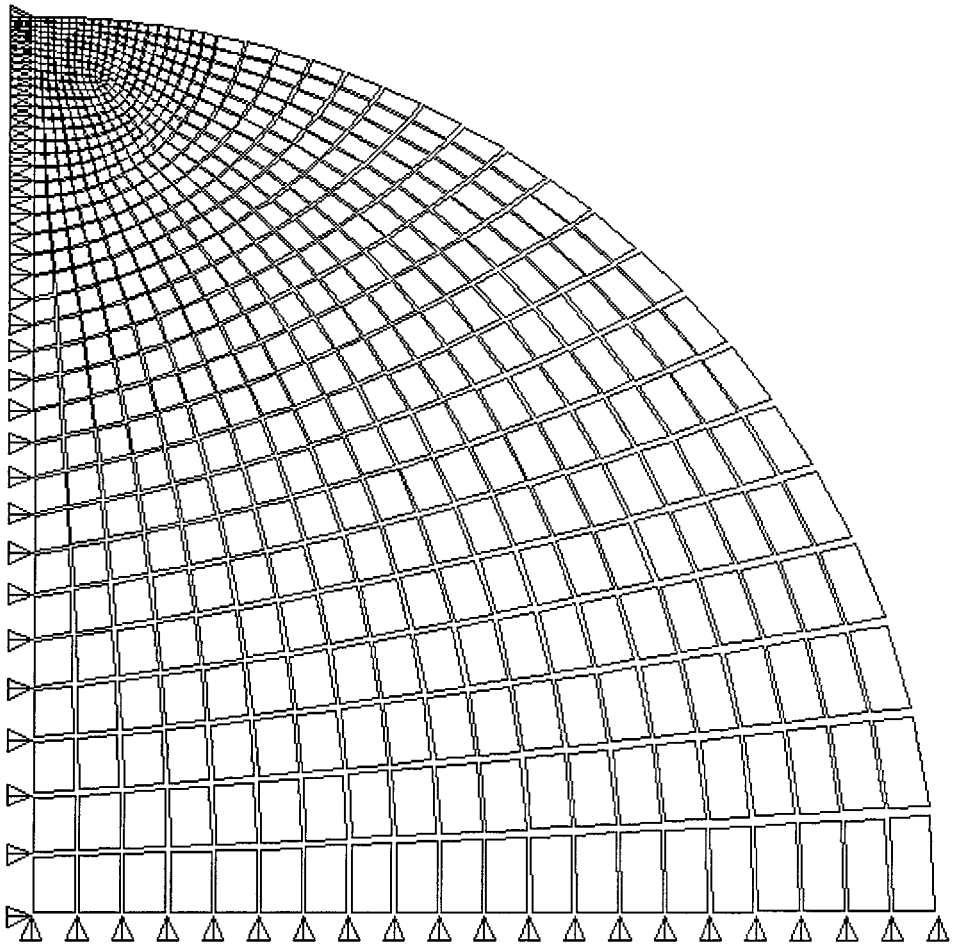

Figure 2 FE model. Example of FE mesh used in simulation of plane strain SFTCT, showing boundary condition (platen, above fiber, not shown). Due to symmetry, only one quarter of the fiber cross-section was modeled.

4. Results

4.1. Force-deflection patterns

SFTCT on PPTA and M5 fibers fell into three distinct force-deflection patterns, shown in Figs 3–5.

The most common behavior was pattern 1 (Fig. 3): upwardly concave initial deformation which resembled Hertzian contact mechanics predictions [2, 13], with an inflection point attributed to yield [2, 29, 19, 38] at $e \approx 5$–10%. From the Hertzian model, the effective transverse modulus was found to be $E_t = 0.75$–3 GPa. Pattern 1 occurred in about 2/3 of tests on each of the continuous filaments tested, and corresponds with previous reports of the transverse compression of PPTA and other, highly-oriented polymer fibers in [2, 29, 19, 38]. The next most common behavior in continuous filaments was pattern 2 (Fig. 4). Pattern 2 was similar to pattern 1, but there was significant scatter in the force-deflection curve soon after yield, often beginning immediately after the inflection point. The most common response in staple fibers was pattern 3 (Fig. 5). Initial deformation was upwardly concave, in qualitative agreement with Hertzian contact predictions for the transverse compression of a homogeneous cylinder, but had more concavity than Hertzian models [2, 13] predict. At some deformation between $10 \geq e \geq 20\%$, response stiffened suddenly, then yielded, most often smoothly, but sometimes erratically. Fitting Equation 1 to initial deformation consistently gave $E_t \approx 0.2$ GPa. Fitting Equation 1 to the stiffest part of the pre-yield response gave spuriously high moduli ($5 < E_t < 15$ GPa). Pattern 3 was also observed in a few tests on continuous filaments. For consistency, pattern 3 data was fitted to Equation 1 on $e < 5\%$.

4.2. Elastic results

Table 1 gives resulting averages for E_t and e_y, from fitting force-deflection data to equation 1. Also given is the maximum resolved shear stress in the cross-section at yield, τ_{max}, from [2]. The large confidence intervals appear to be typical of polymer filaments in SFTCT [39, 30, 31]. Since staple fibers generally had an initial force-deflection curve which was not well-described by equation (1), their resulting E_t should be viewed with caution.

4.3. Confocal microscopy

Figs 6 through 8 show LSCM cross-sections of KEVLAR 29 fibers compressed in SFTCT, to $e = 0$, 25% and 45%, respectively. The fibers appear strongly illuminated at the top (the closest point to the illuminating laser and imaging optics), but to decrease in illumination with increasing depth in y. This may be due to self-reflection and self-absorption of fluorescence in PPTA, however, there is little literature on the subject.

TABLE I SFTCT results. Plus/minus values are 95% confidence intervals

Fiber	Nominal diameter (μm)	No. tests	E_t (GPa)	e_y (%)	τ_{max} (MPa)
Continuous filament					
KEVLAR 29	12	38	2.45 ± 0.40	6.1 ± 1.1	88
KEVLAR 29	24	20	2.38 ± 0.43	3.9 ± 1.1	64
TWARON 1000	12	35	1.70 ± 0.24	7.9 ± 1.2	73
TWARON 1055	12	35	2.11 ± 0.28	8.1 ± 1.2	91
TWARON 2200	12	36	1.59 ± 0.24	7.9 ± 1.5	68
Un-heat-treated M5	12	31	1.37 ± 0.13	5.4 ± 0.5	47
Heat-treated M5	12	41	1.36 ± 0.14	6.0 ± 0.5	49
Staple fiber					
KEVLAR 29	12	13	0.25 ± 0.085		
KEVLAR 29	14	15	0.28 ± 0.082		
KEVLAR 29	20	30	0.70 ± 0.26		
KEVLAR 29	24	33	0.60 ± 0.15		

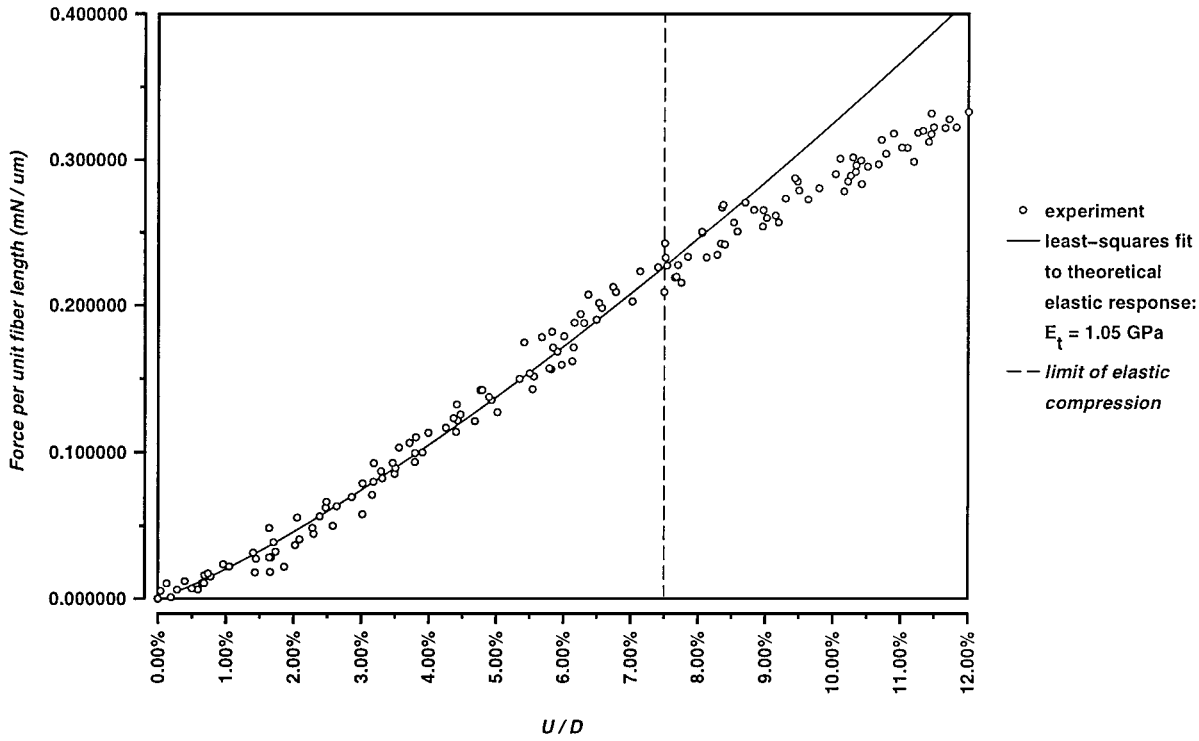

Figure 3 Force-deflection curve pattern 1 (here, heat-treated M5).

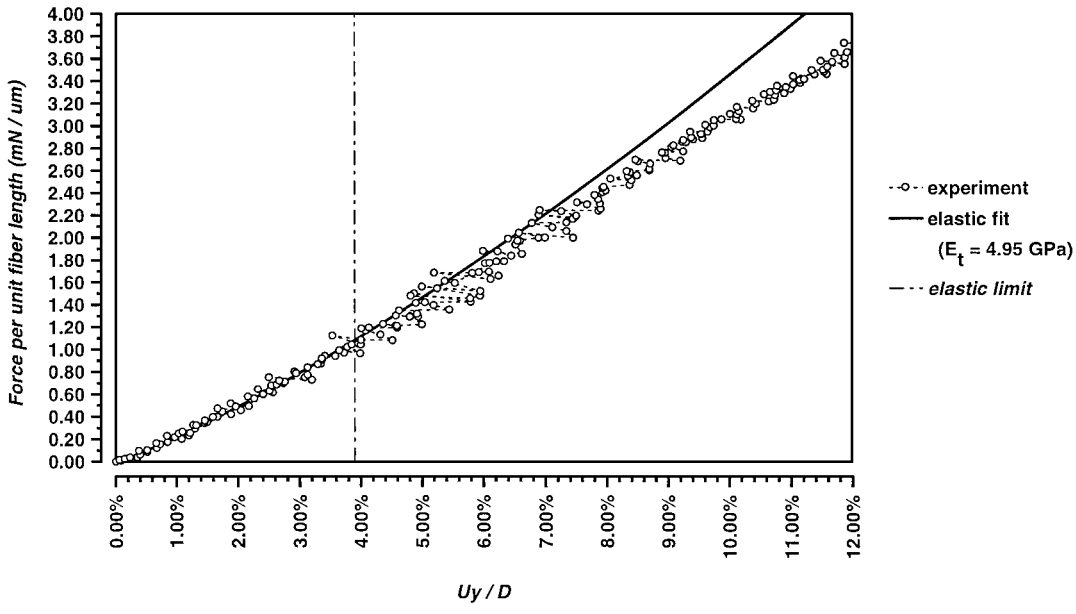

Figure 4 Force-deflection curve pattern 2 (here, TWARON 1000).

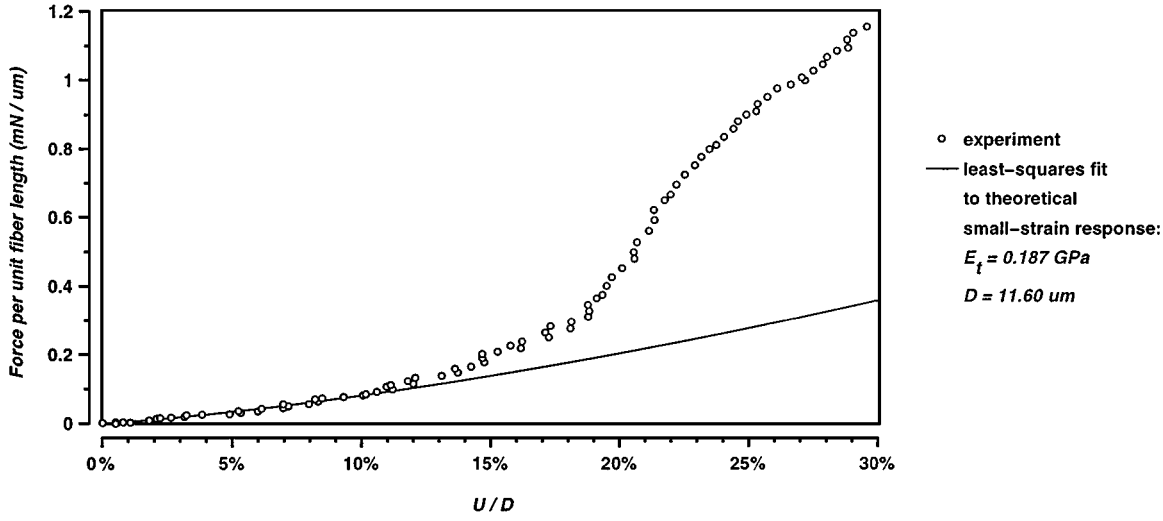

Figure 5 Force-deflection curve pattern 3 (most common in staple fibers; here, 1.5 denier KEVLAR 29 staple fiber).

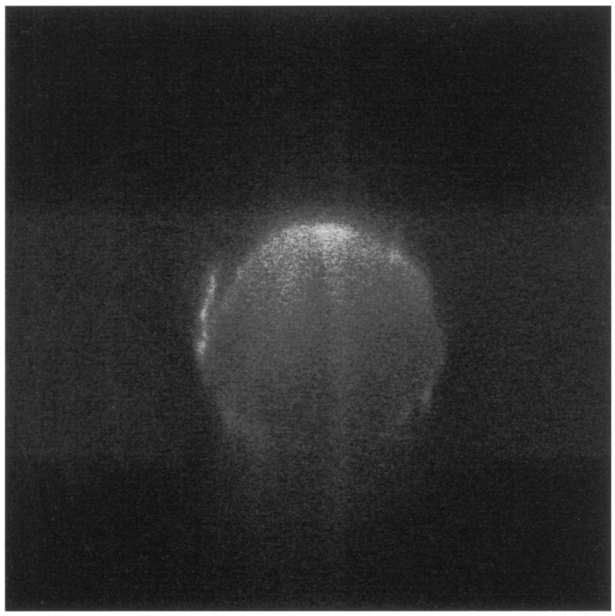

Figure 6 Cross-section of 6 denier untested KEVLAR 29 fiber, imaged by LSCM. Note that only the top surface appears clearly imaged.

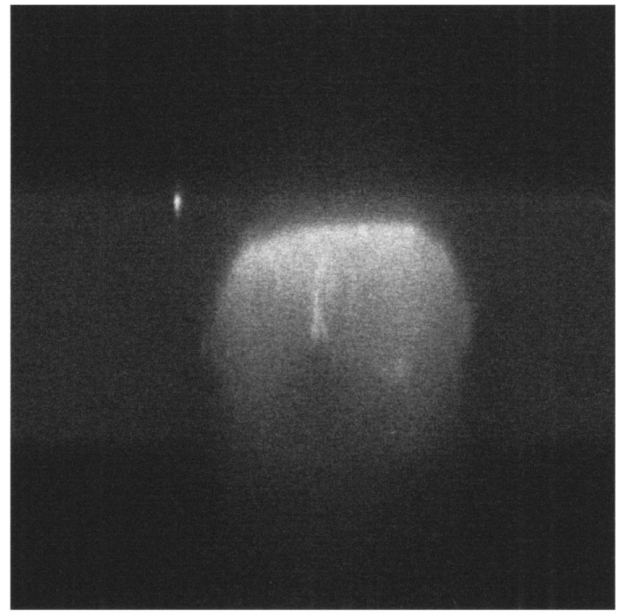

Figure 7 Cross-section of 6 denier KEVLAR 29 fiber, compressed to $e_y \approx$ 25%, imaged by LSCM. Note that only the top surface appears imaged.

The uncompressed cross-section (Fig. 6) appears round, with some small asperities on the fiber surface. Neighboring sections in z showed these to be fibrillated fiber skin, which is seen sporadically in PPTA filaments [40]. The cross-section compressed to $e = 25\%$ (Fig. 7) is race-track shaped, with a flattened top, and no distinguishable features in the fiber interior. This suggests the fiber has deformed inelastically, but without creating any new surface areas for internal reflectance. The cross-section compressed to $e = 45\%$ (Fig. 8) is more extensively flattened, and shows several distinct features in the cross-section. Neighboring sections in z show these are distinct bodies within the fiber, indicating that by $e = 45\%$, fibers have begun to fibrillate.

4.4. FE simulation

Fig. 9 shows an experimental SFTCT force-deflection curve of 1.5 denier KEVLAR 29, and corresponding FE simulation, assuming three different behaviors: perfect elasticity, elastic-perfect plasticity (i.e. $E_{t,\tan} = 0$), and elastic-plastic behavior with some work hardening, $E_{t,\tan} > 0$. The work-hardening simulation agrees with experiment up to $e \approx 30\%$, beyond which element

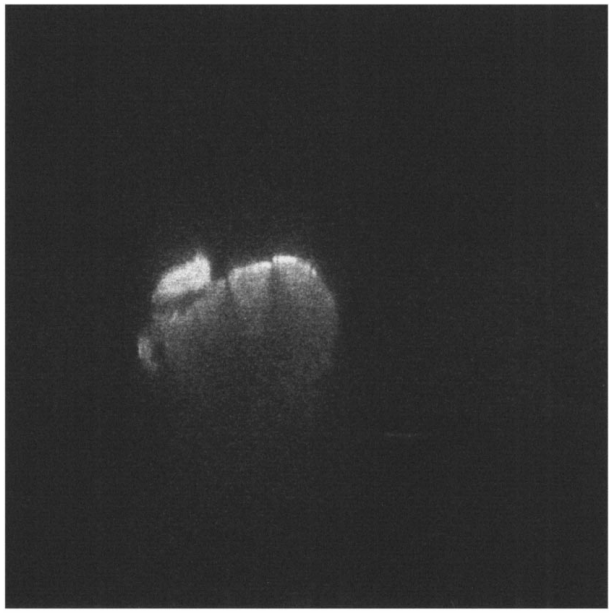

[GLOBAL]
□MethodName=FITC_LP
□DocumentName=
□ImageWidth=512
□ImageLength=512
□NumOfFrames=1

Figure 8 Cross-section of 6 denier KEVLAR 29 fiber, compressed to $e_y \approx$ 45%, imaged by LSCM. Note that only the top surface appears imaged.

distortion in the deforming FE mesh gave convergence difficulties. It appears, however, that if the FE model could continue to converge to higher deformations, it would begin to overpredict experimental force, suggesting another deformation process may occur in PPTA fibers under large compressive strains.

5. Discussion

5.1. Force-deflection patterns

Force-deflection pattern 1 has been reported previously for PPTA [2, 29, 19, 38]. It has been interpreted as Hertzian elastic compression, changing over to plastic yielding at $e_y \approx 6$–8%, starting at the points of maximum shear stress in the cross-section (roughly $[x = 0, 0.7R < |y| < 0.8R]$ [41]), and spreading across the fiber as load increases. Pattern 2 suggests that a minority of PPTA and M5 fibers begin to deform in an erratic, stick-slip process, such as fibrillation, upon or shortly after the onset of yield. Pattern 3, seen predominantly in staple fibers, is clearly not well-described as the plane strain compression of an anisotropic, right circular cylinder. Fig. 10 shows an interpretation of pattern 3, as a cracked fiber, whose cracks close under compression, until the increasing stresses in the fiber cross-section lead to inelastic deformation. That pattern 3 was repeatable suggests the preexisting damage that may have caused it is characteristic of the process of converting KEVLAR 29 filaments into staple fibers.

5.2. Transverse elasticity of PPTA fibers

Heat treating PPTA fibers consistently increases axial modulus, E_l, due to increased crystallinity and axial orientation [9]. Heat treatment has not been consistently found to increase E_t: Phoenix and Skelton [2] and Kawabata [29] found no significant difference between E_t of un-heat-treated and heat-treated KEVLAR. Jones *et al.* [38] found E_t of KEVLAR 49 increased

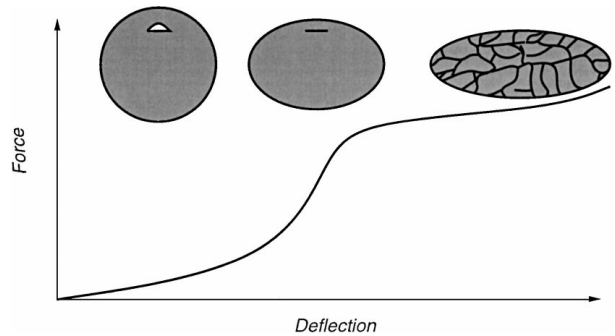

Figure 10 Interpretation of pattern 3 force-deflection curves.

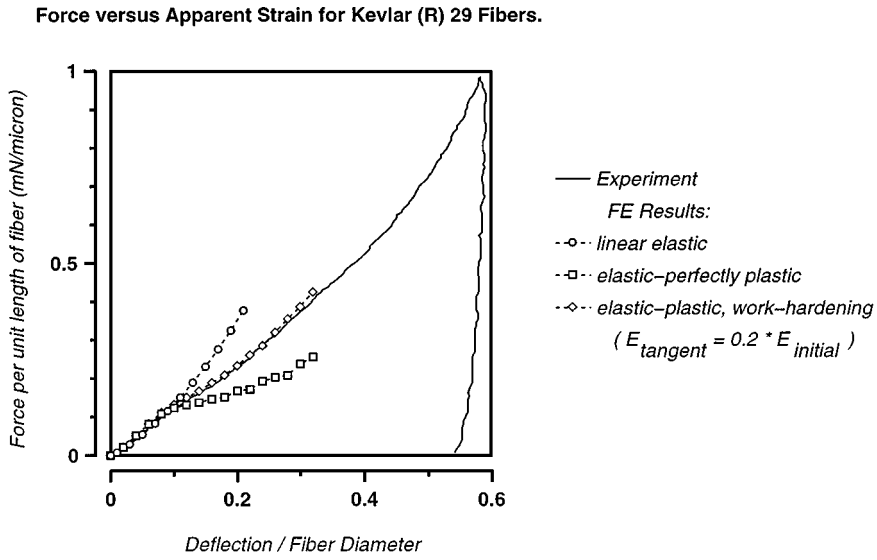

Figure 9 SFTCT force-deflection curve for 1.5 dpf KEVLAR 29 in transverse compression, and FE simulation which assumed perfectly elastic, elastic-perfectly plastic, and elastic-plastic with work hardening.

significantly between KEVLAR 29 and 49, however, their force-deflection data (Fig. 8 in their paper) suggests at least one of the two tests used to determine E_t was pattern 3, for which curve-fitting Equation 1 is somewhat arbitrary. Knoff [19] found significant increase in E_t of KEVLAR 29 after very long heat treatments (1 hour at 250 °C), and moderate increases for faster post treatments. We found heat-treatment moderately increased E_t in TWARON 1055, but did not significantly affect E_t in TWARON 2200, in qualitative agreement with Knoff.

M5 fibers are theorized to form hydrogen bonds in a three-dimensional lattice network [5], in contrast to the planar hydrogen bonding of PPTA. M5 composites have a significantly higher axial compressive strength, which is attributed to this hydrogen bond lattice [6]. Given this, it is surprising that M5 fibers are transversely more compliant than commercial PPTA. Kawabata [29] observed that E_t increases with increasing anisotropic ratio, E_l/E_t, in highly-oriented polymer fibers. Our results for M5 contradict this observation. The low transverse stiffness of M5 fibers may be due to defects in the cross-section, such as voids [28]. The heat treatment applied to M5 fibers had no effect on their elastic response.

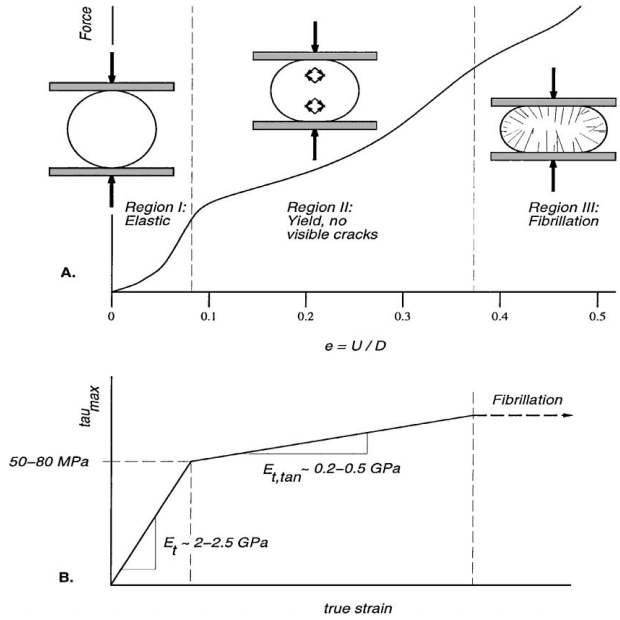

Figure 11 Model of transverse compression response of PPTA fibers. (A) Progression of deformation mechanisms as function of deformation. (B) Corresponding yield criterion.

5.3. Transverse inelasticity of PPTA fibers

The PPTA and M5 fibers examined here yield and deform ductilely in transverse compression at $e_y = 6$–8%, close to apparent yield strains reported previously [29, 19, 38]. Phoenix and Skelton [2] hypothesized yield in PPTA was controlled by the maximum resolved shear stress, τ_{max}. FE simulation which includes von Mises plasticity can reproduce experimental SFTCT force-deflection curves to $e \approx 30\%$, indirectly supporting this hypothesis. Scatter in SFTCT force-deflection data after yield (pattern 2), and LSCM both suggest transverse compressive yield is not always homogeneous deformation; after sufficient transverse deformation, PPTA fibers begin to fibrillate.

LSCM images of 6.0 denier KEVLAR 29 fibers which had pattern 1 force-deflection curves showed no visible cracks at $e = 25\%$, but visible cracks at $e = 45\%$. This suggests flow typically transitions to fibrillation between $e = 20\%$ and 45% (Fig. 11A). After fibrillation, the fiber can support transverse compression and friction-induced shear between disbonded entities, but not tension.

Fig. 9 and SFTCT force-deflection curves for PPTA in previous papers [38, Fig. 8], [19, Fig. 2] showed a second inflection point near $e = 30$–40%, less pronounced than the inflection point at the transition between elastic and inelastic deformation around $e = 6$–8%. This second inflection point may correspond to the onset of visible fibrillation in transversely compressed PPTA fibers. It is smaller than the first inflection point because the difference in effective stiffness (in compression) between fibrillated material and yielded material is smaller than the difference in stiffness between E_t and $E_{t,tan}$. Fig. 11B plots a phenomenological model of the un-heat-treated PPTA yield criterion in transverse compression. Transverse stiffness in Region I is $E_t = 2$–2.5 GPa. The fiber yields at a maximum resolved shear stress of $\tau_{max} = 50$–80 MPa (Region II), with a post-yield modulus of $E_{t,tan} = 0.2$–0.5 GPa. At $e = 30$–40%, the fiber begins to fibrillate. Experimental force-deflection curves of KEVLAR 29, 49 and 149 in [29] suggest $E_{t,tan}$ decreases with increasing heat treatment.

This hypothesis explains most (pattern 1) of the continuous filament tests. Pattern 2 behavior suggests a minority of fibers do not yield significantly before transitioning to fibrillation. This may be due to local defects: superposing the stress concentrations of voids or similar defects on the constitutive relation hypothesized in Fig. 11B could allow disbonding and fibrillation at lower global stresses.

5.4. Skin-core effects of PPTA

Numerous observations [11, 26, 20, 25, 27, 17] have found a radially dependent structure in PPTA fibers, which was not accounted for in the SFTCT analysis. Many researchers have approximated this gradient as a discrete skin and core. Reported skin thickness varies with the experimental method used, but are on the order of 1 μm (compared to a fiber radius of 6 μm). The crystal alignment [25], size and perfection [11, 16, 17] of PPTA fibers are higher near the fiber surface than the core, resulting in lower diffusion coefficients near the skin [27]. These observations suggest PPTA fiber skin is stiffer transversely than the core. We found un-heat-treated KEVLAR was stiffer transversely than un-heat-treated TWARON: if PPTA skin is stiffer transversely than the core, our observation would agree with Dobb and Robson [20], who found TWARON has a thinner skin than KEVLAR. It would also agree with SFTCT findings of Kawabata [29], who found KEVLAR 29 is stiffer transversely than KEVLAR 119, which has a thinner skin. A radial dependence of elastic constants could be incorporated into FE or other simulation of SFTCT (cf. [42, 43]), to simulate its effects on at least elastic

response, if the radial dependence was quantified in the literature: such simulation was not pursued in this study.

5.5. The in-plane anisotropy and structure of PPTA fibers

PPTA fibers are not truly transversely isotropic as assumed in the SFTC analysys, but rather cylindrically orthotropic [44]. Orientation in the fiber cross-section arises from during quenching, when the hydrogen bonds tend to align radially [45, 22]. The consequences of ignoring this in-plane anisotropy in SFTCT analysis need to be determined. Unfortunately, directly determining the mechanical anisotropy in the cross-section of PPTA fibers appears intractable: fiber response to transverse load comes from some average of the in-plane stiffness constants: the normal moduli E_r and E_θ, Poisson's ratio $\nu_{r\theta}$ and the in-plane shear modulus $G_{r\theta}$, all of which are independent.

Radial orientation [14, 46, 15] is not perfect in PPTA fibers, so fiber in-plane anisotropy should be less than the *ab*-plane anisotropy of PPTA crystals. Interference microscopy [15] suggests that, at least optically, KEVLAR 29 fibers are substantially less anisotropic in the cross-section than are the *ab*-plane of PPTA crystals. This suggests the assumption of transverse isotropy is reasonable for at least un-heat-treated PPTA. Ade and coworkers [47, 46] found radial orientation near the fiber skin in KEVLAR fibers increased with increasing heat treatment.

Since PPTA fibers are highly crystalline and highly oriented [9], it is reasonable to estimate the in-plane mechanical anisotropy of PPTA fibers from predictions of the elasticity of PPTA crystals, by assuming the fiber is a polycrystalline assemblage, and taking the appropriate Voigt (stiffness-averaged) or Reuss (compliance-averaged) bounds, as suggested by Rutledge and Suter [24]. In [24], PPTA fibers were assumed transversely isotropic. If instead, the in-plane orientation were assumed not random, but based on experimental measurements (for instance, via interference microscopy as suggested in [15]), the mechanical anisotropy in the cross-section of actual, PPTA fibers could be estimated.

In the assumed transverse isotropy case, Rutledge and Suter [24] found this approach lead to predictions of the two, transversely isotropic fiber Poisson's ratios, ν_{lt} and ν_{tt} which closely agreed with experimental results on high volume fraction composites [33], further, their axial and torsional moduli, E_l and G_{lt}, were only 2-3 times above experimental values for KEVLAR 29 and 49 [48, 33, 38], which could reasonably be attributed to crystalline axial misalignment and intercrystalline defects, respectively. Unfortunately, neither their predictions of the elasticity of PPTA crystals,[2] nor those in [49, 50, 51, 38] lead to predictions of E_t remotely close to experimental results here and elsewhere, instead predicting lower bounds of $13 < E_t < 19$ GPa for PPTA fibers.

[2] There is a typographical error in Table V of [24]. The lower bound prediction is $E_t = 17$ GPa for their structure 3, the Northolt polymorph.

This discrepancy suggests the theoretical elastic constants of PPTA crystals presented in the literature so far have no clear relation to the experimental behavior of PPTA fibers. Further, given the relative accuracy of theoretical predictions of the other elastic constants of an assumed transversely isotropic fiber, it suggests that the transverse deformation of PPTA fibers is strongly limited by compliant defects in the cross-section, much more strongly than either axial stiffness E_l or torsional stiffness G_{lt}. If this is true, then fibrillation under large transverse deformation may be simply the visible, large-scale deformation of a material failing in thin, compliant bands between stiff, crystalline regions which comprise the majority of the cross-section. This would agree with the conclusion reached by McGarry and Moalli [40] after their tests on the tearing strength of KEVLAR 49 fibrils.

We did not attempt to identify the components of the proposed compliant regions in the cross-sections of PPTA: previous investigations have suggested poorly-oriented, intercrystalline regions [16, 11] and/or voids [49, 20, 52, 21, 53], partially filled with entrapped water [19] and quenching impurities [18].

6. Conclusions

Experimental results are presented for the transverse modulus of KEVLAR 29, TWARON 1000, 1055 and 2200, heat-treated and un-heat-treated M5 continuous filaments, as well as KEVLAR 29 staple fibers. There appears to be characteristic damage imparted into staple fibers which makes them more transversely compliant than equivalent PPTA fibers. PPTA fiber appear to yield homogeneously at apparent strains of $e = 6$–8%, but begin to fibrillate at $e = 30$–40%. Indirect evidence suggests the skin of PPTA fibers is stiffer transversely than the core. The transverse stiffness of PPTA is five to ten times lower than lower bound predictions based on the Reuss average of atomistic models of PPTA crystals, which is a substantially greater factor than Reuss average predictions for fiber axial or torsional stiffness. This suggests that the transverse deformation of PPTA fibers depends much more strongly on defects than do axial or torsional response.

Acknowledgements

We gratefully acknowledge the support of DuPont, who paid for this research by a Fellowship Grant, and supplied the SFTCT device and fiber samples. Dr. Li Lin, DuPont Marshall Labs, gave significant help with the SFTCT device. Mr. Patrick Murphy, Akzo Nobel Linear TEnsion Members, and Dr. Maurice Northolt, Akzo-Nobel Central Research, provided samples of TWARON and M5, respectively. We are grateful to Dr. Subhash Batra, NCSU, Dr. Mohan Srinivasarao, Georgia Institute of Technology, and Alex Bogdanovich, 3Tex, for helpful discussions.

References

1. J. SINGLETARY, H. DAVIS, M. K. RAMASUBRAMANIAN, W. KNOFF and M. TONEY, *J. Mater. Sci.* **35** (2000) 573.

2. S. L. PHOENIX and J. SKELTON, *Textiles Research Journal* **65** (1974) 934–940.
3. S. LEIGH PHOENIX, Transverse mechanical behavior of an unimpregnated KEVLAR 29 cable under uniform radial loading. Technical report N66604-74-C-0318, Naval Underwater Systems Center, Purchase Division, Bldg. 126T, Newport, RI, 02840, June 1974.
4. D. J. SIKKEMA, *J. Mater. Sci.* **39**(24) (1998) 5981–5986.
5. E. A. KLOP and M. LAMMERS, *ibid.* **39**(24) (1998) 5987–5998.
6. M. LAMMERS, E. A. KLOP, M. G. NORTHOLT, and D. J. SIKKEMA, *ibid.* **39**(24) (1998) 5999–6005.
7. R. S. PORTER, M. TAKAYANAGI, J. ECONOMY and B. HARRIS, In "High Modulus Polymers and Composites," edited by C. L. Choy, The Chinese University Press, International Summer School at the Chinese University of Hong Kong, (1984) pp. 89–112.
8. *Idem.*, Processing and mechanical properties, in "High Modulus Polymers and Composites," edited by C. L. Choy, The Chinese University Press. International Summer School at the Chinese University of Hong Kong (1984) pp. 113–139.
9. H. H. YANG, KEVLAR, "*Aramid Fiber* (John Wiley & Sons New York, 1989).
10. M. G. NORTHOLT and D. J. SIKKEMA, "Advances in Polymer Science," vol. 98 (Springer-Verlag, Berlin, 1991), chapter 3, pp. 115–177.
11. R. J. MORGAN, C. O. PRUNEDA and W. J. STEELE, *Journal of Polymer Science: Polymer Physics Edition* **21** (1983) 1757–1783.
12. P. SMITH and Y. TERMONIA, *Polymer Communication* **30** (1989) 66–69.
13. S. A. JAWAD and I. M. WARD, *J. Mater. Sci.* **13** (1978) 1381–1387.
14. K. YABUKI, H. ITO and T. OTA, *Sen-I Gakkaishi* **32**(2) (1976) T55–T61.
15. H. DAVIS, J. SINGLETARY, M. SRINIVASARAO, W. KNOFF and M. K. RAMASUBRAMANIAN, *unknown journal*, in preparation.
16. M. PANAR, P. AVAKIAN, R. C. BLUME, K. H. GARDNER, T. D. GIERKE and H. H. YANG, *Journal of Polymer Science, Polymer Physics Edition* **21**(10) (1983) 1955–1969.
17. S. F. Y. LI, A. J. MCGHIE and S. L. TANG, *Polymer* **34**(21) (1993) 4573–4575.
18. R. J. MORGAN and C. O. PRUNEDA, *Polymer* **28** (1987) 340–346.
19. W. F. KNOFF, in Basic Properties of Fibers and Fiber Assemblies, Performance and Design of New Fibrous Materials: Proceedings of the 21st Textile Research Symposium, Fuji Kyouiku Kenshusho (Fuji Educational Training Center), Susono City, Shizuoka, August 7–9, 1992. (Fibrous Materials Research Group, Kyoto University and The Textile Machinery Society of Japan) pp. 5–9.
20. M. G. DOBB and R. M. ROBSON, *J. Mater. Sci.* **25** (1990) 459–464.
21. M. G. DOBB, C. R. PARK and R. M. ROBSON, *ibid.* **27** (1992) 3876–3878.
22. G. C. RUTLEDGE, U. W. SUTER and C. D. PAPASPYRIDES, *Macromolecules* **24** (1991) 1934–1943.
23. G. C. RUTLEDGE and U. W. SUTER, *ibid.* **24** (1991) 1921–1933.
24. *Idem.*, *Polymer* **32**(12) (1991) 2179–2189.
25. R. J. YOUNG, D. LU, J. DAY, W. F. KNOFF and H. A. DAVIS, *J. Mater. Sci.* **27** (1992) 5431–5440.
26. L.-S. LI, L. F. ALLARD and W. C. BIGELOW, *Journal of Macromolecular Science—Physics Edition*, **B22**(2) (1983) 269–290.
27. M. FUKUDA and H. KAWAI, *Textile Research Journal* **63**(4) (1993) 185–193.
28. M. G. NORTHOLT, personal communication, Sept. 1998.
29. S. KAWABATA, *Journal of the Textile Institute* **81**(4) (1990) 433–447.
30. S. K. BATRA and S. NURUZZAMAN, *Journal of Polymer Science: Polymer Physics Edition* **13** (1975) 369–386.
31. T. KOTANI, J. SWEENEY and I. M. WARD, *J. Mater. Sci.* **29** (1994) 5551–5558.
32. J. SINGLETARY, Transverse Compression of Poly(paraphenyleneterephthalamide) and Other, Highly-Oriented Fibers. PhD thesis, North Carolina State University, Raleigh, NC, Dec. 1998.
33. S. KAWABATA, M. SERA, T. KOTANI, K. KATSUMA, M. NIWA and C. XIAOXIN, Anisotropic mechanical properties of advanced high performance fibers obtained by single fiber testing system. Technical report, Department of Polymer Chemistry, Kyoto University, Kyoto 606, Japan, April 1993.
34. S. KAWABATA and K. KATSUMA, Anisotropic Viscoelasticity of Aramid Single Fiber with Transverse Creep Measurement and Modeling of Micro Structure, in Basic Properties of Fibers and Fiber Assemblies, Performance and Design of New Fibrous Materials: Proceedings of the 21st Textile Research Symposium, Fuji Kyouiku Kenshusho (Fuji Educational Training Center), Susono City, Shizuoka, Japan, August 7–9, 1992. (Fibrous Materials Research Group, Kyoto University and The Textile Machinery Society of Japan) pp. 1–4.
35. ANSYS, Inc. Southpointe, 275 Technology Drive, Canonsburg, PA 15317.
36. Swanson Analysis Systems, Inc., PO Box 65, Johnson Road, Houston, PA 15342-0065. *ANSYS User's Manual Volume I: Procedures*, 1992. Revision 5.0.
37. J.-Å. SCHWEITZ. *MRS Bulletin* **17**(7) (1992) 34–45.
38. M.-C. G. JONES, E. LARA-CURZIO, A. KOPPER and D. C. MARTIN, *J. Mater. Sci.* **32** (1997) 2855–2871.
39. D. W. HADLEY, I. M. WARD and J. WARD, *Proceedings of the Royal Society A* **285** (1965) 275–286.
40. F. J. MCGARRY and J. E. MOALLI, *Polymer* **32**(10) (1991) 1811–1815.
41. R. BEECHING and W. NICHOLLS, in *The Institution of Mechanical Engineers Proceedings* (The Institution of Mechanical Engineers, Storey's Gate, St. James Park, London, S.W. 1, 1948) pp. 317–323.
42. B. L. DHOOPAR and P. K. SINHA, *Fibre Science and Technology* **19** (1983) 179–194.
43. T. S. DAVISON, H. N. G. WADLET and M.-J. PINDERA, *Composites Engineering* **4**(10) (1994) 995–1009.
44. H. R. BLADES, U.S. Patent no. 3,869,429, 1975.
45. K. HARAGUCHI, T. KAJIYAMA and M. TAKAYANAGI, *Journal of Applied Polymer Science* **23** (1979) 903–914.
46. A. P. SMITH and H. ADE, *Applied Physics Letters* **69**(25) (1996) 3833–3835.
47. H. ADE and B. HSIAO, *Science* **262**(26) (1993) 1427–1429.
48. W. KNOFF, *J. Mater. Sci.* **22** (1987) 1024.
49. M. G. NORTHOLT and J. J. VAN AARTSEN, *Journal of Polymer Science: Polymer Symposium* **58** (1977) 283–296.
50. X. YANG and S. L. HSU, *Macromolecules* **24** (1991) 6680–6685.
51. D. J. LACKS and G. C. RUTLEDGE, *ibid.* **27** (1994) 1197–1204.
52. M. G. DOBB, C. R. PARK and R. M. ROBSON, *J. Mater. Sci.* **25** (1990) 829–834.
53. J. ECONOMY and K. GORANOV, "Advances in Polymer Science," vol. 17 (Springer-Verlag, Berlin, 1994) chapter 5, pp. 222–257.

Received 18 February
and accepted 12 July 1999